Available online at www.sciencedirect.com
ScienceDirect
International Journal of Thermal Sciences 46 (2007) 358–370
International Journal of Thermal Sciences
www.elsevier.com/locate/ijts

Radiation effect on thermal explosion in a gas containing evaporating fuel droplets

I. Goldfarb [a], V. Gol'dshtein [a], D. Katz [a,*], S. Sazhin [b]

[a] *Department of Mathematics, Faculty of Natural Sciences, Ben Gurion University of the Negev, Grossman Building, P.O.B. 653, Beer Sheva 84105, Israel*
[b] *School of Engineering, Faculty of Science and Engineering, University of Brighton, Cockcroft Building, Brighton BN2 4GJ, UK*

Received 11 August 2005; received in revised form 27 June 2006; accepted 27 June 2006

Available online 28 August 2006

Abstract

The dynamics of thermal explosion in a fuel droplets/hot air mixture is investigated using the geometrical version of the method of integral manifolds. The results are applied to the modelling of the ignition process in diesel engines. Effects of the thermal radiation, semi-transparency of droplets and oxidizer are taken into account. In contrast to the previous studies, the difference between gas temperature (responsible for convective heating of droplets) and external temperature (responsible for radiative heating of droplets) is taken into account. The dynamics of the explosion is presented in terms of the dynamics of a multi-scale, singularly perturbed system. The relevant parametric regions of this system are analyzed. Explicit analytical formulae for the ignition delay in the presence of thermal radiation are derived. It is shown that the effect of thermal radiation can lead to considerable reduction (up to about 30%) of the total ignition delay time.

Keywords: Diesel fuel; Combustion; Thermal explosion; Thermal radiation

1. Introduction

The practical importance of the problem of a thermal explosion in a mixture containing fuel droplets and gas is well known and it has been widely discussed in literature (e.g. [1,2]). In most cases this problem has been studied based on the application of computational fluid dynamics (CFD) packages [2]. One of the benefits of this approach is that it could take into account the complicated geometry of the enclosure and chemistry of the processes involved. This makes it particularly attractive for engineering applications including the modelling of combustion processes in diesel engines. In this case, the thermal explosion is modelled alongside a number of other processes, including turbulence and the effects of complicated geometry. This inevitably obscures the underlying physical processes involved, and is likely to mitigate the limitations of the physical and chemical models.

Alternative approaches to the problem are based on the asymptotic analysis of equations describing the limiting cases of the processes. Although these approaches cannot replace the conventional CFD analysis, they can effectively complement it. One of these approaches is based on the application of the zero-order approximation of the geometric version of the asymptotic Method of Integral Manifolds (MIM), developed for combustion applications in [3,4]. The results of the application of this method have been reported in a number of papers. In [5] this approach was applied to a specific problem of modelling of ignition process in diesel engines. The radiative energy exchange between the fuel droplet surfaces and gas was described using the P-1 model. The chemical term was presented in the Arrhenius form with the pre-exponential factor calculated from the enthalpy equation, using the Shell autoignition model. The ignition process was subdivided into two stages: droplet evaporation and ignition of the gaseous mixture. Results predicted by the analytical solutions were compared with those predicted by the CFD package VECTIS. The effects of thermal radiation were shown to be significant, especially at high temperatures and for large droplets. There were a number of limitations of the model used in that paper. A simplified thermal radiation model

* Corresponding author.
E-mail addresses: goldfrab@cs.bgu.ac.il (I. Goldfarb), vladimir@math.bgu.ac.il (V. Gol'dshtein), katsda@math.bgu.ac.il (D. Katz), s.sazhin@brighton.ac.uk (S. Sazhin).

1290-0729/$ – see front matter
doi:10.1016/j.ijthermalsci.2006.06.014

Nomenclature

a	coefficient introduced in Eq. (6) ..... m^{-b}
a_i, $i = 0, 1, 2$	coefficients introduced in Eq. (6).. $m^{-b}\,K^{-i}$
af, bx	coefficients used in the definition of $\dot{\omega}$
A	pre-exponential factor ..... $kmol^{1-(af+bx)}\,m^{3-3(af+bx)}\,s^{-1}$
b	coefficient introduced in Eq. (7)
b_i, $i = 0, 1, 2$	coefficients introduced in Eq. (7) ..... K^{-i}
C	molar concentration ..... $kmol\,m^{-3}$
c	specific heat capacity ..... $J\,kg^{-1}\,K^{-1}$
E	activation energy ..... $J\,kmol^{-1}$
F, G	functions introduced in Eqs. 8 and 9
h	convection heat transfer coefficient .. $W\,m^{-2}\,K^{-1}$ or position of the manifold
k_1	efficiency factor of absorption
L	latent heat of evaporation ..... $J\,kg^{-1}$
M	molar mass ..... $kg\,kmol^{-1}$
n	number of droplets per unit volume ..... m^{-3}
p	pressure ..... Pa
P_i, $i = 1, 2, 3$	dimensionless components of the RHS of system (1)–(5)
q	heat flux ..... $W\,m^{-2}$
Q	specific combustion energy ..... $J\,kg^{-1}$
r	dimensionless droplet radius
R_d	droplet radius ..... m
R	universal gas constant ..... $J\,kmol^{-1}\,K^{-1}$
t	time ..... s
T	temperature ..... K
$\vec{v}$	phase velocity vector defined by Eq. (10)
x, y	arguments introduced in Eqs. (8)–(9)

Greek symbols

β	E/RT_{d0}
β_i	E/RT_{db}
γ	small dimensionless parameter
δ	impact of the thermal radiation ..... %
ε_i, $i = 1, 2, 3, 4$	dimensionless parameters introduced in Eqs. (11)–(15)
ε	small positive parameter introduced in Eq. (9)
η	dimensionless fuel concentration
θ	dimensionless gas temperature
ζ	parameter introduced in Eqs. (2) and (5)
λ	thermal conductivity ..... $W\,m^{-1}\,K^{-1}$
ν	stoichiometric coefficient
ξ	dimensionless oxidizer concentration
ρ	density ..... $kg\,m^{-3}$
σ	Stefan–Boltzmann constant ..... $W\,m^{-2}\,K^{-4}$
τ	dimensionless delay time
φ	dimensionless volumetric phase content
ω	small dimensionless parameter
$\dot{\omega}$	chemical reaction rate ..... $kmol\,s^{-1}$
Ω	RHS of the slow curve equation

Subscripts

b	boiling point
c	convection
d	droplet
ext	external
f	fuel
fs	saturated fuel vapour
g	gas mixture
gf	final of gas mixture
hp	heat-up
i	induction
ox	oxidizer
p	constant pressure
r	thermal radiation
react	reaction
0	initial state

Superscripts

C	convective
CR	convective and radiative
ext	external

was used, based on the assumption that droplets are opaque grey spheres. The droplet heat-up period was not considered. The model was tested for 'average' values of parameters in a diesel engine combustion chamber, and the dependence of the results on the variations of parameters there was not investigated. The analytical part of the analysis was based on the assumption that there was no deficiency of oxygen in the system, which can hardly be justified for the region in the immediate vicinity of the nozzles.

Some of the limitations of the model used in [5] were overcome in [6]. The model for the radiative heating of droplets, used in the latter paper, took into account the semi-transparency of droplets, but it was assumed that gas in diesel engines is optically thick. This allowed the authors to assume that the radiation temperature is equal to the gas temperature. A simplified model for droplet heat-up was used. As in [5] it was assumed that oxygen is not deficient in the system. The analysis was limited to just 2 sets of parameters, typical for the diesel engine environment. These are 'far zone' (small initial liquid volume fraction and small droplet radii) and 'near zone' (large initial liquid volume fraction and large droplet radii). The conditions of the first zone were typical for the areas in the diesel engine combustion chamber which are far from the fuel injectors, while the conditions of the second zone were typical for the areas in the combustion chamber which were relatively close to the fuel injectors. It was pointed out that droplets heating and evaporation time in the far zone was smaller than the chemical ignition delay of the fuel vapour/air mixture. The total ignition delay decreased when the initial gas temperature increased. In the near zone, the process started with the initial gas cooling and slight heating of droplets. This was followed by a relatively slow heating of gas due to the chemical reaction, and further

droplet heating. The total ignition delay in the near zone was larger than in the far zone. It was expected that before thermal explosion in the near zone takes place, the droplets break up and are removed from this zone. Effects of thermal radiation in both zones were shown to be negligible for small droplets but were noticeable for large droplets.

In this paper the models described in [5,6] are developed further and applied to the realistic conditions in diesel engines. As in [6], the effects of thermal radiation are taken into account, the droplets are assumed to be semi-transparent, and a simplified radiation absorption model described in [7,8] is used. In contrast to [6], however, the radiation temperature is identified with the external temperature. This is a more realistic situation for diesel engines where this external temperature can be identified with the temperature of remote flames. The modelling of the heat-up process is similar to the one used in [6]. It is based on the model suggested in [9]. In contrast to that paper, however, the deficiency of oxygen is taken into account. The applicability of the method of integral manifolds in various regions in diesel engines is investigated. The analytical expressions for the total ignition delay are obtained, where appropriate. The classification of possible thermal regimes of the system is suggested.

2. Basic equations and approximations

Spray ignition is considered as an explosion problem, where droplets are regarded as the source of endothermicity. The endothermic versus exothermic competition determines explosion regimes and their dependence on the physical and chemical parameters of the system. The medium is modelled as a spatially homogeneous mixture of an optically thin, combustible gas with a mono-dispersed spray of evaporating fuel droplets. The distortion of the incident radiation by surrounding droplets, the effects of droplet movement and the effect of temperature gradient inside droplets are ignored. It is assumed that the incident radiation has a black-body spectrum. The system is assumed to be adiabatic. The limitations of these assumptions and the range of their applicability have been discussed in numerous papers, including [10–13].

With a view to the application of the results to diesel engines, we assume that gas pressure is constant. Both convective and radiative heating of droplets are taken into account. The thermal conductivity of the liquid phase is assumed to be infinitely large.

The volume fraction of the liquid phase is assumed to be much less than that of the gaseous phase. Thus, the heat transfer coefficient of the mixture is controlled by the thermal properties of the gaseous component. It is assumed that the burning process, described by the first order exothermic reaction, takes place in the gaseous phase only. Droplet velocities and the effects of natural convection are neglected in the analysis. Therefore, ignoring the effects of the Stefan flow, Nusselt (Nu) and Sherwood (Sh) numbers are taken equal to 2.

These assumptions allow us to describe the system by the following equations:

$$c_{pg}\rho_g\varphi_g\frac{\mathrm{d}T_g}{\mathrm{d}t} = \dot{\omega}M_f Q_f\varphi_g - 4\pi R_d^2 n_d q_c \tag{1}$$

$$\frac{\mathrm{d}C_f}{\mathrm{d}t} = -\nu_f\dot{\omega} + 4\pi R_d^2 n_d\frac{(q_c+q_r)}{LM_f\varphi_g}\big(1-\zeta(T_d)\big) \tag{2}$$

$$\frac{\mathrm{d}C_{ox}}{\mathrm{d}t} = -\nu_{ox}\dot{\omega} \tag{3}$$

$$c_f m_d\frac{\mathrm{d}T_d}{\mathrm{d}t} = 4\pi R_d^2(q_c+q_r)\zeta(T_d) \tag{4}$$

$$\frac{\mathrm{d}}{\mathrm{d}t}\left(\frac{4}{3}\pi R_d^3\rho_f\right) = -4\pi R_d^2\frac{(q_c+q_r)}{L}\big(1-\zeta(T_d)\big) \tag{5}$$

where

$$\dot{\omega} = C_f^{af}C_{ox}^{bx}A\exp\left(-\frac{E}{RT_g}\right)$$

$$q_c = h_c(T_g-T_d),\qquad h_c = \frac{\lambda_g}{R_d}$$

$$q_r = k_1\sigma T_{\mathrm{ext}}^4,\qquad k_1 = aR_d^b$$

$$a = a_0 + a_1\left(\frac{T_{\mathrm{ext}}}{10^3}\right) + a_2\left(\frac{T_{\mathrm{ext}}}{10^3}\right)^2 \tag{6}$$

$$b = b_0 + b_1\left(\frac{T_{\mathrm{ext}}}{10^3}\right) + b_2\left(\frac{T_{\mathrm{ext}}}{10^3}\right)^2 \tag{7}$$

$$\zeta(T_d) = \frac{T_b-T_d}{T_b-T_{d0}}$$

The initial conditions are the following: $T_d|_{t=0} = T_{d0}$, $T_g|_{t=0} = T_{g0}$, $R_d|_{t=0} = R_{d0}$, $C_f|_{t=0} = C_{f0}$, $C_{ox}|_{t=0} = C_{ox0}$. The external thermal radiation is assumed to be that of a black body, with the temperature T_{ext}. The values of parameters used in the calculations are given in Section 3.3.

3. Analysis and results

The analysis of Eqs. (1)–(5) is based on the geometrical version of the method of integral manifolds (MIM), which leads to a simple, yet informative and practically useful description of the system dynamics. In the next subsection Eqs. (1)–(5) are presented in the dimensionless form and basic principles of their analysis are described. In Section 3.3 possible dynamic scenarios described by this system are analyzed. It is shown that this system can be treated as singularly perturbed in two cases: when gas or droplet temperatures are fast variables. These two cases are analyzed in detail in Sections 3.4 and 3.5.

3.1. Method of integral manifolds

Method of integral manifolds (MIM) is described in details in [14,15]. The original geometrical version of this method was applied to stiff problems of chemical kinetics and combustion by Gol'dshtein and Sobolev [4]. To demonstrate the essence of this approach, let us consider a 2-dimensional system of ordinary differential equations:

$$\frac{\mathrm{d}x}{\mathrm{d}t} = F(x,y) \tag{8}$$

$$\varepsilon\frac{\mathrm{d}y}{\mathrm{d}t} = G(x,y) \tag{9}$$

where $F(x, y)$ and $G(x, y)$ are continuous functions of their arguments. If the parameter ε is small ($0 < \varepsilon \ll 1$), then system (8)–(9) is called singularly perturbed.

In such case, curve $M := \{(x, y)\colon\ y = h(x, \varepsilon)\}$ is defined as an integral manifold of Eqs. (8)–(9).

If any phase trajectory $\gamma(x, y)$ of these equations intersecting with M belongs to M in the domain of existence of M [16]. The general theory of integral manifolds states that integral (invariant) manifolds M belong to the ε-neighborhood of the slow (quasi-stationary) manifold $M_0 := \{(x, y)\colon\ y = h_0(x)\}$, where $y = h_0(x)$ is an isolated solution of Eq. (9) with $\varepsilon = 0$. It was shown in [14,15] that the slow surface (slow manifold) M_0 is an $O(\varepsilon)$ approximation of the integral manifold, which can be used for qualitative analysis. This allows us to lower the dimension of the system under investigation.

At each point of the phase space (or at each point of the region where system (8)–(9) is considered), this system determines the phase-velocity vector:

$$\vec{v}(x, y) = \left(\frac{1}{\varepsilon}G(x, y), F(x, y)\right) \tag{10}$$

which is tangential to the system trajectory.

The slow manifold may attract or repel system trajectories. This is determined by the direction of vector field (10): toward the slow surface or away from it.

Each trajectory of the system under consideration in the close vicinity of the slow surface tends to some trajectory on the slow surface. The slow parts of the trajectory are located on M. Its stability is controlled by the sign of $\frac{\partial G}{\partial x}$. The conditions $\frac{\partial G}{\partial x} < 0$ and $\frac{\partial G}{\partial x} > 0$ define the stable (attractable) and unstable (repealing) manifolds, respectively. The condition for marginal stability $F = \frac{\partial F}{\partial x} = 0$ defines the above mentioned turning points, which separate the stable (attractable) parts from the unstable (repelling) parts.

For the purpose of qualitative analysis, the zero approximation, M_0, of the system integral manifold can be taken. This means that the application of the technique presented above to the solution of Eqs. (8)–(9) should start with an estimate of the relative rates of change of the variables and a decision as to which of them are fast and which are slow.

3.2. Dimensionless system

Following Semenov [17] we have introduced the following dimensionless variables:

$$\theta_g = \frac{E}{RT_{d0}}\frac{T_g - T_{d0}}{T_{d0}}, \qquad \theta_d = \frac{E}{RT_{d0}}\frac{T_d - T_{d0}}{T_{d0}}$$

$$r = \frac{R_d}{R_{d0}}, \qquad \eta = \frac{C_f}{C_{ff}}, \qquad \xi = \frac{C_{ox}}{C_{ox0}}$$

where

$$\tau = \frac{t}{t_{\text{react}}}, \quad t_{\text{react}} = \frac{1}{AC_{ff}^{af-0.5}C_{ox0}^{bx-0.5}}\exp\left(\frac{1}{\beta}\right)$$

The initial conditions for dimensionless variables are:

$$\theta_g\big|_{\tau=0} = \theta_{g0} \neq 0, \qquad \theta_d\big|_{\tau=0} = \theta_{d0} = 0$$

$$r|_{\tau=0} = r_0 = 1, \qquad \eta|_{\tau=0} = \eta_0, \qquad \xi|_{\tau=0} = \xi_0 = 1$$

Using these dimensionless variables, Eqs. (1)–(5) can be rewritten as:

$$\frac{d\theta_g}{d\tau} = \frac{1}{\gamma}\big(P_1(\theta_g, \eta, \xi) - P_2(\theta_g, \theta_d, r)\big) \tag{11}$$

$$\frac{d\eta}{d\tau} = \frac{1}{\tilde{\nu}_f}\left[-P_1(\theta_g, \eta, \xi) + \frac{\psi}{\nu_f}P_{23}(\theta_g, \theta_d, r)\big(1 - \zeta(\theta_d)\big)\right] \tag{12}$$

$$\frac{d\xi}{d\tau} = -\frac{1}{\tilde{\nu}_{ox}}P_1(\theta_g, \eta, \xi) \tag{13}$$

$$\frac{d\theta_d}{d\tau} = \frac{\varepsilon_2}{\varepsilon_4 r^3}\big(P_2(\theta_g, \theta_d, r) + P_3(r)\big)\zeta(\theta_d) \tag{14}$$

$$\frac{d(r^3)}{d\tau} = -\varepsilon_2\big(P_2(\theta_g, \theta_d, r) + P_3(r)\big)\big(1 - \zeta(\theta_d)\big) \tag{15}$$

where

$$\beta = \frac{RT_{d0}}{E}, \qquad \gamma = \frac{c_{pg}T_{d0}\rho_g\beta}{(C_{ox0}C_{ff})^{0.5}Q_f M_f}$$

$$C_{ff} = \frac{4\pi}{3}R_{d0}^3\rho_f n_d\frac{1}{M_f}(1 + \omega_f), \quad \omega_f \ll 1$$

$$\varepsilon_1 = \frac{4\pi R_{d0}n_d\lambda_{g0}T_{d0}\beta}{C_{ff}^{af}C_{ox0}^{bx}AQ_f\varphi_g M_f}\exp\left(\frac{1}{\beta}\right)$$

$$\varepsilon_2 = \frac{(C_{ox0}C_{ff})^{0.5}Q_f\varphi_g M_f}{\rho_f L\varphi_f}$$

$$\varepsilon_3 = \frac{4T_{d0}^3\sigma R_{d0}k_{10}}{\lambda_{g0}}, \qquad \varepsilon_4 = \frac{c_f T_{d0}\beta}{L}$$

$$P_1(\theta_g, \eta, \xi) = \eta^a\xi^b\exp\left(\frac{\theta_g}{1 + \beta\theta_g}\right)$$

$$P_2(\theta_g, \theta_d, r) = \varepsilon_1 r\sqrt{\frac{T_{d0}(1 + \beta\theta_g)}{T_{g0}}}(\theta_g - \theta_d)$$

$$P_3(r) = \frac{\varepsilon_1\varepsilon_3}{4\beta}r^{2+b}\big(1 + \beta\theta_g^{\text{ext}}\big)^4$$

$$P_{23}(\theta_g, \theta_d, r) \equiv P_2(\theta_g, \theta_d, r) + P_3(r)$$

$$\theta_g^{\text{ext}} = \frac{1}{\beta}\frac{T_{\text{ext}} - T_{d0}}{T_{d0}}, \qquad \zeta(\theta_d) = \frac{T_b - T_{d0}(1 + \beta\theta_d)}{T_b - T_{d0}}$$

$$\tilde{\nu}_f = \frac{1}{\nu_f}\sqrt{\frac{C_{ff}}{C_{ox0}}}, \qquad \tilde{\nu}_{ox} = \frac{1}{\nu_{ox}}\sqrt{\frac{C_{ox0}}{C_{ff}}}$$

Appropriate combination of Eqs. (14)–(15) yields the partial integral of this system in the form:

$$r(\theta_d) = \sqrt[3]{\big(e^{\theta_d}\cdot\big(\zeta(\theta_d)\big)^{\theta_{db}}\big)^{\varepsilon_4}} \tag{16}$$

As follows from expression (16), $r \to 0$ when $\zeta \to 0$. The latter happens when the droplet surface temperature approaches the boiling temperature. In addition, expression (16) allows us to exclude Eq. (15) from the following investigation.

In order to clarify the influence of the thermal radiation on the delay time before the final explosion of the system we introduce the term *impact of the thermal radiation*, which is measured in per cents and defined as:

$$\delta(\%) = \frac{\tau_{\text{delay}}^{\text{CR}} - \tau_{\text{delay}}^{\text{C}}}{\tau_{\text{delay}}^{\text{CR}}}\cdot 100 \tag{17}$$

where $\tau_{\text{delay}}^{\text{CR}}$ and $\tau_{\text{delay}}^{\text{C}}$ are the delay times obtained from Eqs. (11)–(14) and (16) with and without taking into account the influence of thermal radiation. In the latter case we assume that $P_3 = 0$.

3.3. Possible dynamical scenarios

The system has been analyzed for the set of parameters typical for diesel engines [5]:

$E = 7.6 \times 10^7\ \text{J kmol}^{-1}$

$\lambda_{g0} = 0.061\ \text{W m}^{-1}\,\text{K}^{-1}$

$T_{d0} = 300\ \text{K}$

$c_{pg} = 1120\ \text{J kg}^{-1}\,\text{K}^{-1}$

$M_f = 170\ \text{kg kmol}^{-1}$

$T_{\text{ext}} = 2500\ \text{K}$

$Q_f = 4.3 \times 10^7\ \text{J kg}^{-1}$

$\sigma = 5.67 \times 10^{-8}\ \text{W m}^{-2}\,\text{K}^{-4}$

$T_b = 600\ \text{K}$

$\rho_{g0} = 23.8\ \text{kg m}^{-3}$

$L = 3.6 \times 10^5\ \text{J kg}^{-1}$

$\rho_f = 600\ \text{kg m}^{-3}$

$a_0 = 0.104\ \text{m}^{-b}$

$a_1 = -0.05432\ \text{m}^{-b}\,\text{K}^{-1}$

$a_2 = 0.008\ \text{m}^{-b}\,\text{K}^{-2}$

$b_0 = 0.49162$

$b_1 = 0.098369\ \text{K}^{-1}$

$b_2 = -0.007857\ \text{K}^{-2}$

The values of physical parameters, except for the spectral properties, are taken for n-dodecane. The spectral properties are based on direct measurements for low sulphur ESSO AF1313 diesel fuel as reported in [8].

The values of the initial gas temperatures, droplet radii and droplet concentrations are taken in the range:

$$(T_{g0}, R_{d0}, n_{d0}) \in [600, 1100] \times \left[5 \times 10^{-6}, 5 \times 10^{-5}\right] \times \left[10^6, 10^{12}\right] \tag{18}$$

where T_{g0} is in K, R_{d0} is in m and n_{d0} is in m^{-3}.

Note that not all combinations of the parameters shown above can be observed in diesel engines. For example, the assumption that spherical non-interacting droplets are present in the gas is expected to be valid only when their volume fraction is small enough. Assuming that this threshold value is 0.3 we can write this condition in the form:

$$\varphi_f = \frac{4\pi}{3} R_{d0}^3 n_{d0} < 0.3$$

The plots of R_{d0} versus n_{d0} for $\varphi_f = 0.0001, 0.001, 0.01, 0.1$ and 0.3 (numbers near the curves) are shown in Fig. 1. The range of parameters for which $\varphi_f > 0.3$ corresponds to the shaded area on this figure.

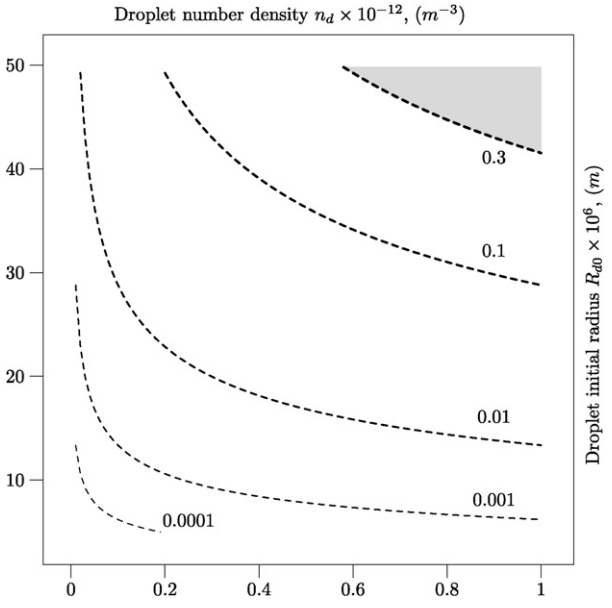

Fig. 1. Plots of droplet radii versus droplet number density for various φ (indicated near the curves). The parametric domain where $\varphi_f > 0.3$ is shown in the top right corner.

For the process under consideration, the system of governing equations is given by Eqs. (11)–(15). The explosive process described by these equations represents a sequence of subprocesses. The fastest subprocess is called fast. Every fast subprocess is characterized by the highest rate of change of the variables. The rate of change of system variables at every stage of the process is determined by the absolute values of the right-hand sides of the corresponding equations. Hence, in order to determine which of the system variables is the fastest at the initial stage of the process, the absolute values of the right-hand sides of the governing equations at $\tau = 0$ will be analyzed. This will allow us to identify possible dynamic regimes of the system and link them to sub-ranges of parameters. Eqs. (11)–(15) have no discontinuities, but they are highly non-linear. To identify the boundaries of various dynamic regimes of the system, the following mesh-based algorithm is used.

The 3-dimensional parametric domain (18), describing the range of possible values of T_{g0}, R_{d0} and n_{d0}, is divided into smaller boxes, such that the length of each of their side is one hundredth of the appropriate initial box side length. Let us denote

$$H_i = H_i(T_{g0}, R_{d0}, n_{d0}), \quad i = 1, \ldots, 4 \tag{19}$$

as the initial *absolute* value of the right-hand side of one of Eqs. (11)–(14) ($i = 1, 2, 3, 4$ refers to Eqs. (11)–(14), respectively). The values of variables θ_g, η, ξ, θ_d and r in the right-hand sides of these equations are taken equal to their initial values. The initial absolute value of the right-hand side of Eq. (15) is equal to 0.

Let

$$H_{ij} = \frac{H_i(T_{g0}, R_{d0}, n_d)}{H_j(T_{g0}, R_{d0}, n_d)}, \quad i, j = 1, \ldots, 4,\ i \neq j \tag{20}$$

The values of H_{ij} were arranged into four arrays:

$$H^1 = \{H_{12}, H_{13}, H_{14}\} \quad (21)$$

$$H^2 = \{H_{21}, H_{23}, H_{24}\} \quad (22)$$

$$H^3 = \{H_{31}, H_{32}, H_{34}\} \quad (23)$$

$$H^4 = \{H_{41}, H_{42}, H_{43}\} \quad (24)$$

A variable of the system is considered to be the fastest if, for a given combination (T_{g0}, R_{d0}, n_{d0}), all components of the appropriate array are greater than 10. As follows from our analysis, for certain initial gas temperatures and droplet concentrations, elements of Array (21), satisfying this condition for the dimensionless gas temperature, are restricted from below by a certain threshold initial droplet radius. The plots of allowed minimum R_{d0} versus T_{g0} for $n_d = 2.8 \times 10^{11}$ m^{-3}, $n_d = 3 \times 10^{11}$ m^{-3} and $n_d = 4 \times 10^{11}$ m^{-3} are shown in Figs. 2, 3 and 4, respectively. In the unshaded areas above the plots shown in these figures, the dimensionless gas temperature θ_g is the system fast variable. Note that the values of R_{d0} are limited from above by the condition $\varphi_f < 0.3$ (see Fig. 1) and the upper limit for R_{d0} observed in diesel engines (see Eq. (18)). Comparing Figs. 2, 3 and 4, one can see that the range of allowed values of R_{d0} widens with increasing values of n_d.

Similarly, the maximal values of R_{d0} for which the elements of Array (24) satisfy a similar condition for dimensionless droplet temperatures θ_d for $n_d = 10^{11}$ m^{-3} and $n_d = 2 \times 10^{11}$ m^{-3} are shown in Figs. 5 and 6 respectively, in a certain range of initial gas temperatures. In the unshaded areas shown in these figures, the dimensionless droplet temperature θ_d is the fast system variable. As in Figs. 2, 3 and 4, the values of R_{d0} are restricted from above by the condition $\varphi_f < 0.3$ (see Fig. 1) and the upper limit for R_{d0} observed in diesel engines (see Eq. (18)). They are restricted from below by the lower limit for R_{d0} (see Eq. (18)). As follows from Figs. 5 and 6, the range of allowed values of R_{d0} widens with increasing T_{g0}.

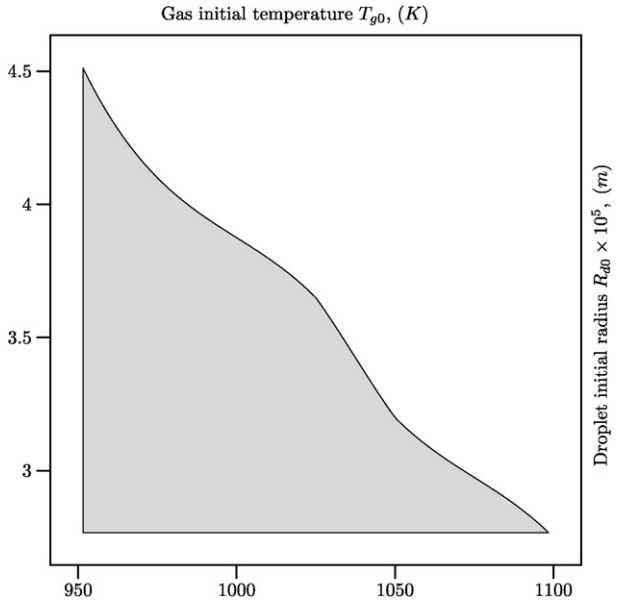

Fig. 2. Plot of the minimal values of R_{d0}, when gas temperature can be considered as the fast variable, versus T_{g0} for $n_d = 2.8 \times 10^{11}$ m^{-3}. The unshaded area corresponds to the fast gas temperature domain.

Domains of the fast gas temperature, shown in Figs. 2, 3 and 4, refer to relatively large droplets injected into a rather hot gas. These conditions can refer to the case of droplets in the vicinity of the nozzle in a diesel engine combustion chamber when the combustion process has already started (recall our earlier assumption that $T_{\text{ext}} = 2500$ K). Domains of the fast droplet temperature, shown in Figs. 5 and 6, refer to smaller droplets injected into cooler gas. In the absence of thermal radiation, this domain can be associated with the region in a diesel engine combustion chamber away from the nozzle (cf. the corresponding regions discussed in [6]). Gas temperatures, slightly lower than those expected at the end of the compression stroke in diesel engines can be attributed to heat consumption during the evaporation process. In the presence of thermal radiation,

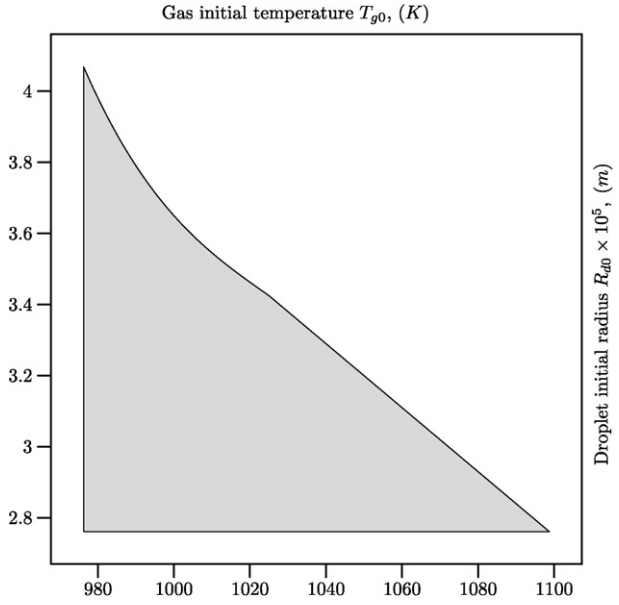

Fig. 3. The same as Fig. 2 but for $n_d = 3 \times 10^{11}$ m^{-3}.

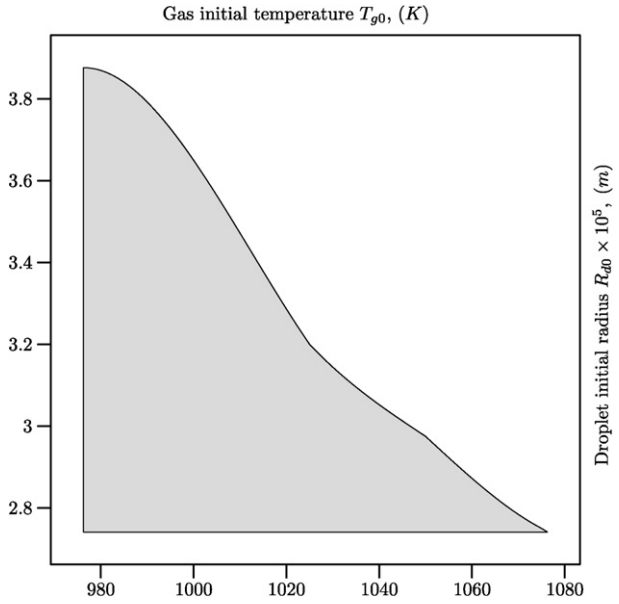

Fig. 4. Fig. 2 but for $n_d = 4 \times 10^{11}$ m^{-3}.

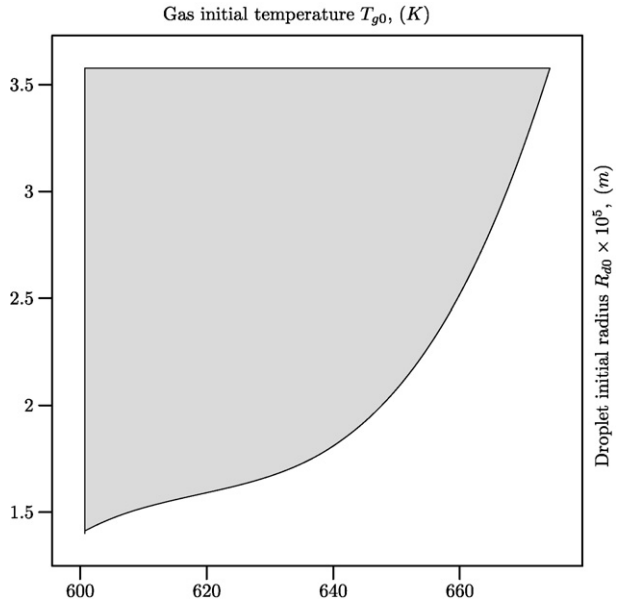

Fig. 5. Plot of the maximal values of R_{d0}, when droplet temperature can be considered as the fast variable, versus T_{g0} for $n_d = 1 \times 10^{11}$ m^{-3}. The unshaded area corresponds to the fast droplet temperature domain.

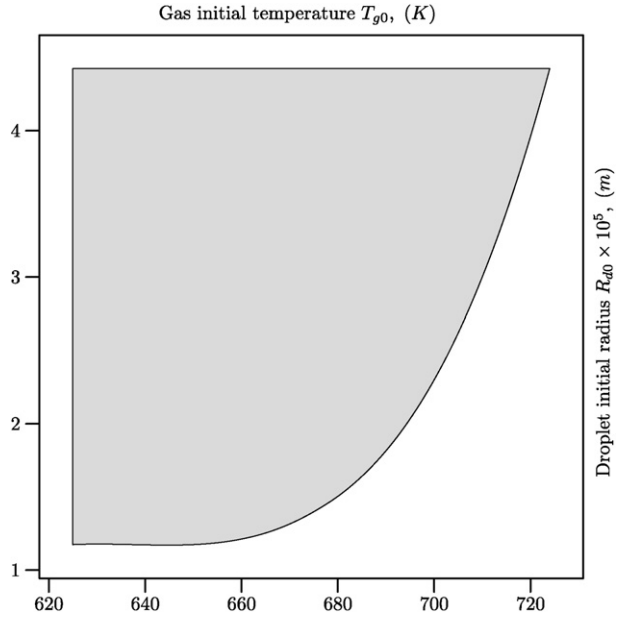

Fig. 6. The same as Fig. 5 but for $n_d = 2 \times 10^{11}$ m^{-3}.

this domain can be associated with the case when the ignition has taken place at one side of the spray, but has not yet spread to the whole spray (see [18,19]).

Arrays (22) and (23) do not satisfy the above mentioned conditions for the values of H_{ij}. This means that, in the given domain (18), the dimensionless fuel concentration η and dimensionless oxidizer concentration ξ cannot be the system fast variables. Hence, we can expect that the only possible dynamical scenarios, when the method of integral manifolds can be applied, are those when the fast dimensionless variables are gas temperature θ_g and droplet temperature θ_d (and normalized droplet radius: see Eq. (16)). These will be considered in detail in the following sections.

3.4. Case A: Fast gas temperature θ_g

This scenario is realized when the initial gas temperature T_{g0}, initial droplet radius R_{d0} and the initial droplets number density n_{d0} have the values in the domains, shown in Figs. 2, 3 and 4. The system slow curve is obtained by setting the right-hand side of Eq. (11) to 0. In the case of one fast and one slow variable, the slow manifold of the system is a two-dimensional curve. In the general case, however, several slow variables can be present in the system. In order to reduce the number of these variables the partial integrals could be used. The system under investigation has just one such integral, which is described by Eq. (16). Its further analysis could be simplified if the slowest variable is found among the slow variables. The task of finding such variable is not difficult, since only the right-hand side of the Eq. (15) is zero when $\tau = 0$. Hence, the slowest system variable at the initial stage of the process is the dimensionless droplet radius r. This can be chosen as the second variable of the system slow curve, i.e.:

$$\Omega(\theta_g, r) = P_1(\theta_g, \eta_0, \xi_0) - P_2(\theta_g, \theta_{d0}, r) = 0$$

As follows from our analysis for the set of parameters under consideration the trajectory of system (11)–(14) lies in the repulsive part of the slow curve. Therefore, the delay time can be formally obtained by the integration of Eq. (11) between the initial, θ_{g0}, and final, θ_{gf}, values of the dimensionless gas temperature:

$$\tau_{\text{delay}} = \gamma \int_{\theta_{g0}}^{\theta_{gf}} \frac{\mathrm{d}\theta_g}{(1+\beta\theta_g)(P_1(\theta_g, \eta_0, \xi_0) - P_2(\theta_g, \theta_{d0}, r_0))} \quad (25)$$

The practical application of Eq. (25) is limited due to the fact that the value of θ_{gf} is not known and needs to be obtained from the numerical solution of the system of Eqs. (11)–(14). Figs. 7 and 8 show the dependence of T_{gf} on the droplets number density n_d. Note that the delay time predicted by Eq. (25) is different from the total ignition delay defined as the time span between droplet injection and the time when the fuel vapour/air mixture reaches an *a priori* chosen temperature (typically 1100 K) [20,21]. The latter is typically used for the analysis of the processes in diesel engines. The dependence of τ_{delay} on the effects of thermal radiation lies in the dependence of θ_{gf} on this radiation (via the term P_3).

Figs. 9 and 10 show the dependence of the delay time on the droplets number density in the presence of thermal radiation for three values of the initial droplet radius ($R_{d0} = 34$ μm, $R_{d0} = 32$ μm, $R_{d0} = 30$ μm) and for two values of the initial gas temperature 1075 K and 1100. These values of parameters together with the assumed value of the external temperature T_{ext} are extreme rather than typical for the diesel engine environment. The external temperature can be associated with the temperature of remote flame. Strong dependence of the delay time on droplet radius is due to the corresponding dependence θ_{gf} on the amount of burnt fuel.

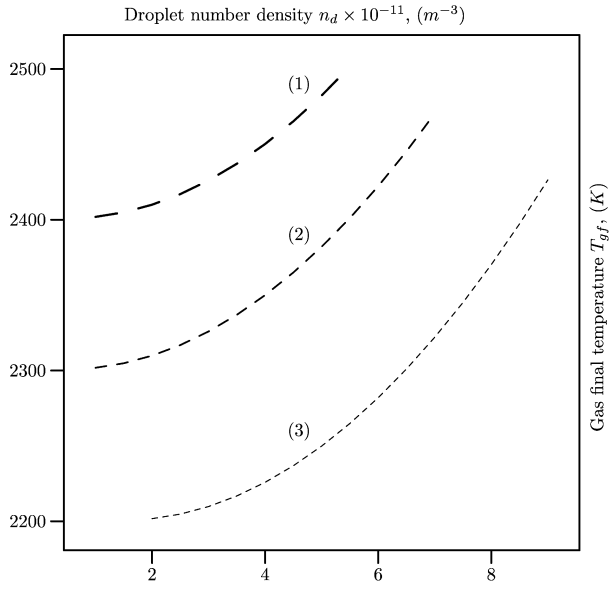

Fig. 7. Gas final temperature T_{gf} versus droplets number density as predicted by Eq. (25), for $T_{\text{ext}} = 2500$ K and $T_{g0} = 1075$ K ((1) refers to $R_{d0} = 34$ μm, (2) refers to $R_{d0} = 32$ μm, (3) refers to $R_{d0} = 30$ μm).

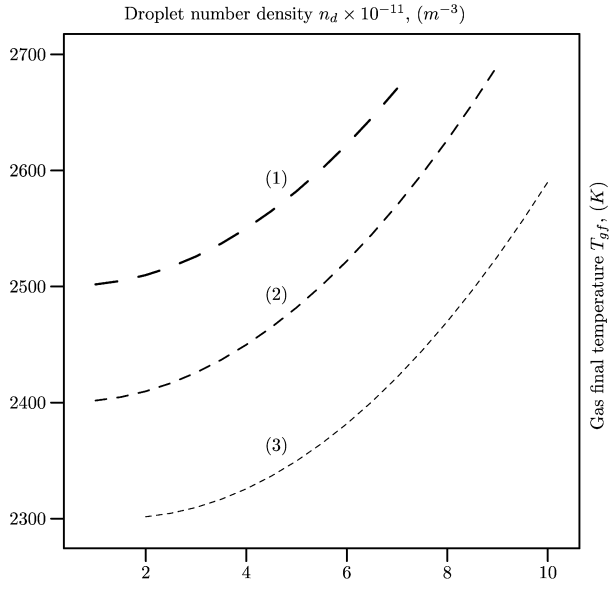

Fig. 8. The same as Fig. 7 but for $T_{g0} = 1100$ K.

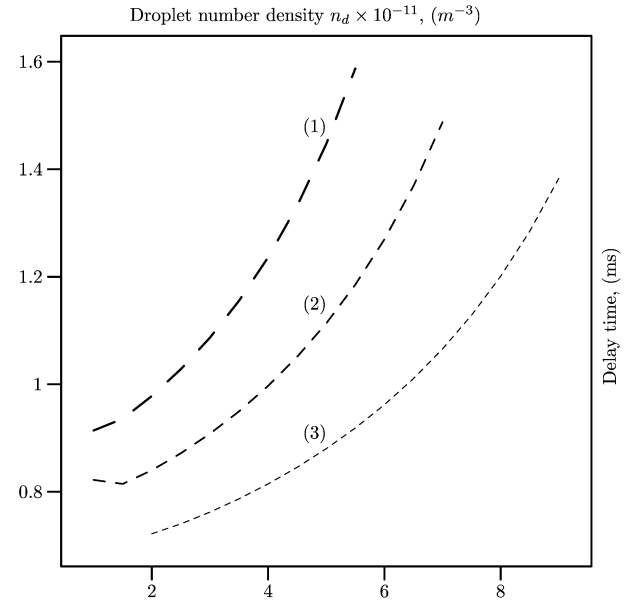

Fig. 9. Delay time versus droplets number density as predicted by Eq. (25) in the presence of thermal radiation, for $T_{\text{ext}} = 2500$ K and $T_{g0} = 1075$ K ((1) refers to $R_{d0} = 34$ μm, (2) refers to $R_{d0} = 32$ μm, (3) refers to $R_{d0} = 30$ μm).

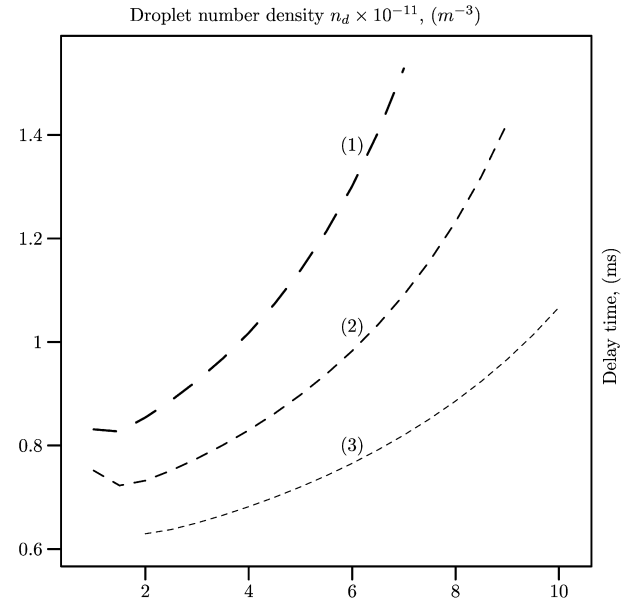

Fig. 10. The same as Fig. 9 but for $T_{g0} = 1100$ K.

As follows from Figs. 9 and 10, the delay times increase with increasing droplet number density and droplet initial radii. This is an expected result, as the ignition delay is ultimately controlled by the rate of increase of gas temperature. If the volume fraction of the liquid fuel is too high then the drop of gas temperature due to droplet evaporation would lead to the additional delay in the setup of the ignition.

Comparing Figs. 9 and 10 one can see that the ignition delay decreases with increasing initial gas temperature. This result is understandable: the higher the initial gas temperature is, the more favorable are the conditions for the oxidizing of fuel, and the shorter is the predicted ignition delay.

The dependence of the radiation impact on the droplet number density is shown in Figs. 11 and 12 for the same values of the initial droplet radii and gas temperatures as in Figs. 9 and 10. The negative impact of thermal radiation shown in Figs. 11 and 12 indicates that the thermal radiation leads to decrease of the ignition delay. This result is expected from the point of view of the underlying physics of the process. The more heat is absorbed by the droplet via thermal radiation—the quicker it is evaporated. The energy for this evaporation, however, is taken mainly from the external source of thermal radiation and not from the surrounding gas. When the number of droplets present in the system and their radii increase, then the amount of ther-

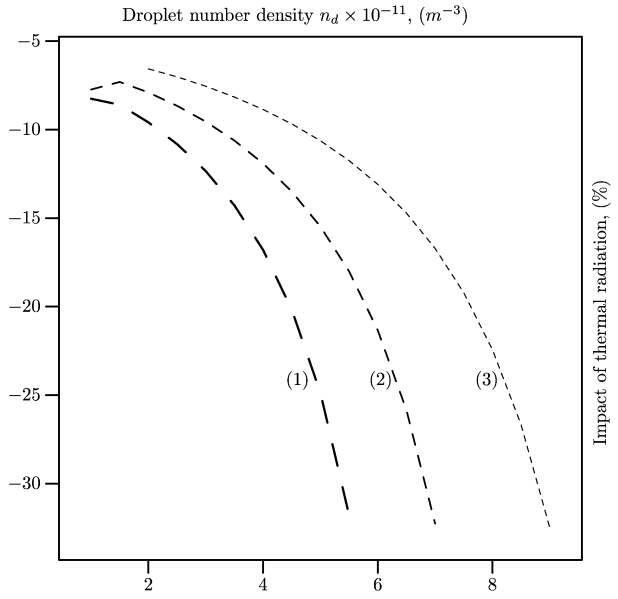

Fig. 11. Impact of thermal radiation versus droplets number density as predicted by Eq. (25), for $T_{\text{ext}} = 2500$ K and $T_{g0} = 1075$ K ((1) refers to $R_{d0} = 34$ μm, (2) refers to $R_{d0} = 32$ μm, (3) refers to $R_{d0} = 30$ μm).

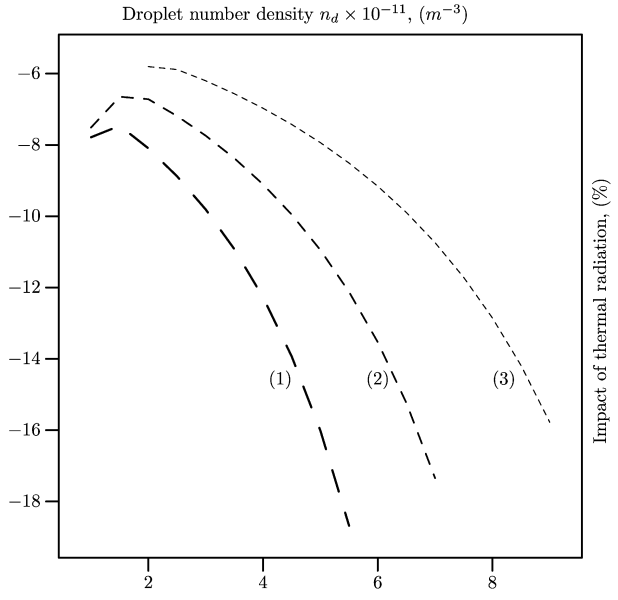

Fig. 12. The same as Fig. 11 but for $T_{g0} = 1100$ K.

mal radiation absorbed by the liquid fuel is expected to increase as well. This is consistent with the increase of thermal radiation impact with increased droplet number density and radii shown in Figs. 11 and 12. A slight decrease of this impact with increasing droplet number density at the initial part of two of the curves shown in Fig. 12, can be attributed to additional gas temperature drop due to enhanced evaporation under the influence of thermal radiation. A decrease of the impact of thermal radiation with increased initial gas temperatures, which can be seen by comparison of Figs. 11 and 12 can be attributed to the increased role of convective heating at higher gas temperatures.

Note that the system dynamics for the case when gas temperature is the fast variable, as described above, is different from the system dynamics for a similar case when gas temperature is the fast variable, as described in [6]. In the latter case, the slow manifold was attractive, and the ignition delay was mainly determined by the time, which the system spent on the slow manifold. Hence the ignition delays predicted by Figs. 9 and 10 turned out to be more that 2 orders of magnitude shorter than that predicted in [6]. This can be attributed to the smaller initial gas temperature 900 (K), and much smaller external temperature used in the analysis of [6]. The latter was assumed equal to T_g, and this led to a much smaller impact of thermal radiation predicted by [6] compared with our current analysis. This result would be expected in the light of the physical background of the processes involved.

Also, the values of the coefficients in the chemical terms used in the present model and in [6] are different. It is rather difficult to compare them, as the used models had different foundations. In the present model the coefficients were taken from [22] and the deficiency of oxygen was taken into account. In [6] the coefficients obtained in [5] were used. These were based on the approximation of the results predicted by the Shell model. Both approaches are rather inaccurate. We cannot, at present, compare the results predicted by our simplistic model with experimental data or CFD calculations (e.g. [18,19]). The main reason for this is that the regime predicted by this model is likely to be realized in the vicinity of the nozzle, where we cannot ignore the inhomogeneity of the medium and the effect of fast moving droplets. Although the ignition delays predicted by the present model are much shorter than those predicted in [6], they are still likely to be shorter than the transit time of droplets in the vicinity of the nozzle (less than about 1 mus). Hence, ignition in this region is not expected. This prediction of the model agrees with available experimental data and the predictions of CFD simulations [18,19].

3.5. Case B: Fast droplet temperature θ_d

This scenario is realized when the initial gas temperature T_{g0}, initial droplet radius R_{d0} and the initial droplets number density n_{d0} are in the domains, shown in Figs. 5 and 6. In this case the thermal explosion process should be divided into two separate consecutive sub-processes: the heat-up and evaporation process and the induction process. The actual time delay before the explosion occurs can be estimated as the sum of the heat-up and evaporation time (physical delay) and the induction time (chemical delay). In the following two sections these times will be estimated separately.

3.5.1. Heat-up and evaporation time

During the heat-up and evaporation period the dimensionless temperature of relatively cold (compared to the surrounding gas) fuel droplets rises from its initial value θ_{d0} to its boiling point θ_b. This heating of droplets is accompanied by their evaporation as predicted by Eq. (16). Since the droplet dimensionless temperature θ_d is the fastest system variable, the rest of the system variables, except for the droplet normalized radius r (which is related to θ_d via Eq. (16)) are assumed constant. Moreover, as mentioned earlier, during the heating process the

fuel droplets evaporate completely (within the droplet heat-up model used in this paper)

Since during the heat-up and evaporation period the droplet dimensionless temperature θ_d is the fastest system variable, the slow curve of the system is obtained by equating the right-hand side of Eq. (14) to 0, i.e.:

$$\Omega(\theta_g,\theta_d)=\frac{\varepsilon_2}{\varepsilon_4 r^3(\theta_d)}\big[\big(P_2\big(\theta_g,\theta_d,r(\theta_d)\big)+P_3\big(r(\theta_d)\big)\big)\zeta(\theta_d)\big]=0 \tag{26}$$

where $r(\theta_d)$ is given by Eq. (16).

The trajectory of the system starts with the fast motion from the initial point $(\theta_{g0},\theta_{d0})$ toward the attractive branch of Slow curve (26). After a short period of time, it intersects with the slow curve at the point which coordinates $(\theta_{g0},\theta_d^\star)$ satisfy the equation of the slow curve:

$$\Omega(\theta_{g0},\theta_d^\star)=0$$

Thereafter, it starts a relatively slow movement along the attractive branch of the slow curve. This movement continues until the trajectory reaches the point $(\theta_{gb},\theta_{db})$, where θ_{gb} is the dimensionless gas temperature corresponding to the dimensionless fuel boiling temperature θ_{db}. This point is the turning point of Slow curve (26). It satisfies the following equations (see Section 3.1):

$$\begin{cases}\Omega(\theta_{gb},\theta_{db})=0\\ \frac{\partial\Omega}{\partial\theta_d}(\theta_{gb},\theta_{db})=0\end{cases}$$

Ignoring the contribution of the initial fast part of the system trajectory, the *heat-up period* can be estimated from the analysis of the part of the trajectory along the attractive branch of the slow curve. Using Eq. (11) we obtain the expression of the heat-up and evaporation period in the form:

$$\tau_{hp}=\int_{\theta_{g0}}^{\theta_{gb}}\frac{\gamma\,\mathrm{d}\theta_g}{(1+\beta\theta_g)(P_1(\theta_g,\eta_0,\xi_0)-P_2(\theta_g,\theta_d,r))} \tag{27}$$

Since the dimensionless variables θ_g and θ_d are on the slow curve, we obtain from Eq. (26): $-P_2(\theta_g,\theta_d,r)=P_3(r)$. In addition, the implicit expressions $\theta_g=\theta_g(\theta_d)$ and $\theta_d=\theta_d(\theta_g)$ can be readily obtained from the same equation. Using Eq. (16), we can write $P_3(r)\equiv P_3(\theta_d)$. This leads to the following formula of the heat-up and evaporation time:

$$\tau_{hp}^{\mathrm{CR}}=\int_{\theta_{g0}}^{\theta_{gb}}\frac{\gamma\,\mathrm{d}\theta_g}{(1+\beta\theta_g)(P_1(\theta_g,\eta_0,\xi_0)+P_3(\theta_g))} \tag{28}$$

where the additional superscript CR indicates that both convective and radiative heating are taken into account. In the absence of thermal radiation this equation is simplified to:

$$\tau_{hp}^{\mathrm{C}}=\int_{\theta_{g0}}^{\theta_{gb}^\star}\frac{\gamma\,\mathrm{d}\theta_g}{(1+\beta\theta_g)P_1(\theta_g,\eta_0,\xi_0)} \tag{29}$$

where superscript C indicates that only convective heating is taken into account, the point $(\theta_{gb}^\star,\theta_{db})$, with $\theta_{gb}\neq\theta_{gb}^\star$, is the turning point of the slow curve

$$\Omega^\star(\theta_g,\theta_d)=\frac{\varepsilon_2}{\varepsilon_4 r^3(\theta_d)}\big[P_2\big(\theta_g,\theta_d,r(\theta_d)\big)\zeta(\theta_d)\big]=0 \tag{30}$$

which can be found from Eqs. (11)–(14).

3.5.2. Induction time

The heat-up and evaporation time, discussed in the previous section, describes the period when droplet dimensionless temperature θ_d reaches its boiling value θ_{db} and the droplets evaporate. As mentioned earlier, during this time the fuel droplets evaporate completely. Therefore, Eqs. (15) and (14) can be excluded from the system of Eqs. (11)–(15). Also, after the droplets have evaporated the heat exchange between the gaseous and liquid phases disappears. Thus, the terms $P_2(\theta_g,\theta_d,r)$, $P_3(\theta_g^{\mathrm{ext}},r)$ and $P_{23}(\theta_g,\theta_g^{\mathrm{ext}},\theta_d,r)$ describing the heat and the thermal radiation fluxes, are to be removed from the system equations under consideration.

We introduce the following new dimensionless variable:

$$\theta_{gi}=\frac{E}{RT_{db}}\frac{T_g-T_{db}}{T_{db}}=\beta_i\frac{T_g-T_{db}}{T_{db}} \tag{31}$$

where $\beta_i=\frac{E}{RT_{db}}$ and T_{db} is the boiling temperature of the fuel.

This allows us to present the system of the governing equations in the form:

$$\frac{\mathrm{d}\theta_{gi}}{\mathrm{d}\tau}=\frac{1+\beta_i\theta_{gi}}{\gamma}P_1(\theta_{gi},\eta,\xi) \tag{32}$$

$$\frac{\mathrm{d}\eta}{\mathrm{d}\tau}=-\frac{1}{\tilde{\nu}_f}P_1(\theta_{gi},\eta,\xi) \tag{33}$$

$$\frac{\mathrm{d}\xi}{\mathrm{d}\tau}=-\frac{1}{\tilde{\nu}_{ox}}P_1(\theta_{gi},\eta,\xi) \tag{34}$$

where

$$\begin{cases}\theta_{gi}|_{\theta_d=\theta_{db}}=\theta_{gi0}\neq 0\\ \eta|_{\theta_d=\theta_{db}}=\eta_b\\ \xi|_{\theta_d=\theta_{db}}=\xi_b=1\end{cases}$$

As in [6], the induction time can be calculated as:

$$\tau_{\mathrm{induction}}=\frac{\gamma}{\eta_b^{af}\xi_b^{bx}}\int_{\theta_{g0}}^{\infty}e^{-\theta_g}\,\mathrm{d}\theta_g=\frac{\gamma}{\eta_b^{af}\xi_b^{bx}} \tag{35}$$

The total ignition delay is calculated as:

$$\tau_{\mathrm{total}}=\tau_{hp}+\tau_{\mathrm{induction}} \tag{36}$$

The plots of the total ignition delay in the presence of thermal radiation, as predicted by Eq. (36), versus droplet number density for two values of the initial droplet radii 12 μm and 9.5 μm are shown in Figs. 13 and 14. These figures refer to the initial gas temperatures 750 K and 775 K. The value of the external temperature is assumed equal to 2500 K. The values of these parameters are chosen in such a way that they satisfy the condition for fast droplet temperature. These values are typical for the diesel engine environment, except for the value of the external temperature. The latter is higher than typically observed,

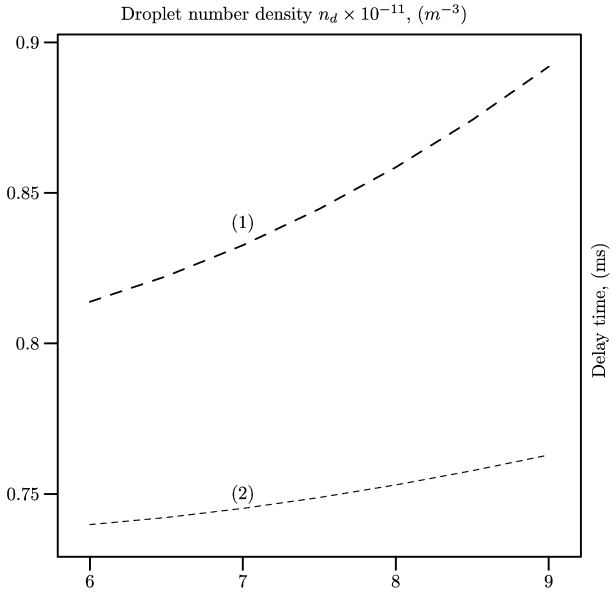

Fig. 13. Total ignition delay time versus droplets number density in the presence of thermal radiation as predicted by Eq. (36) for $T_{\text{ext}} = 2500$ K and $T_{g0} = 750$ K ((1) refers to $R_{d0} = 12$ μm, (2) refers to $R_{d0} = 9.5$ μm).

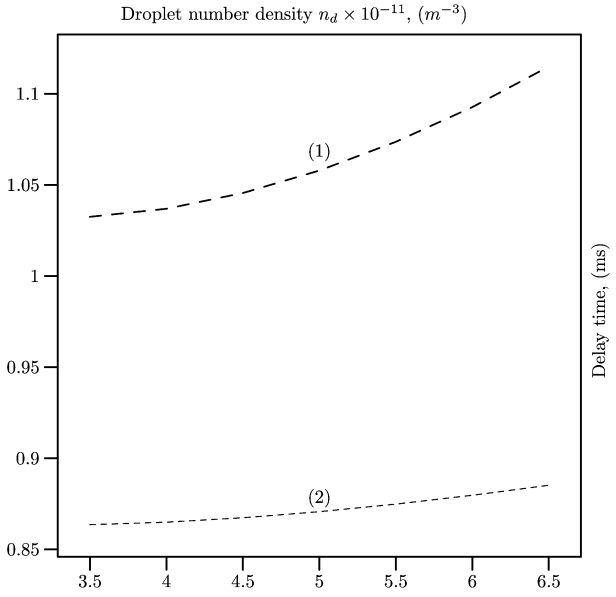

Fig. 14. The same as Fig. 13 but for $T_{g0} = 775$ K.

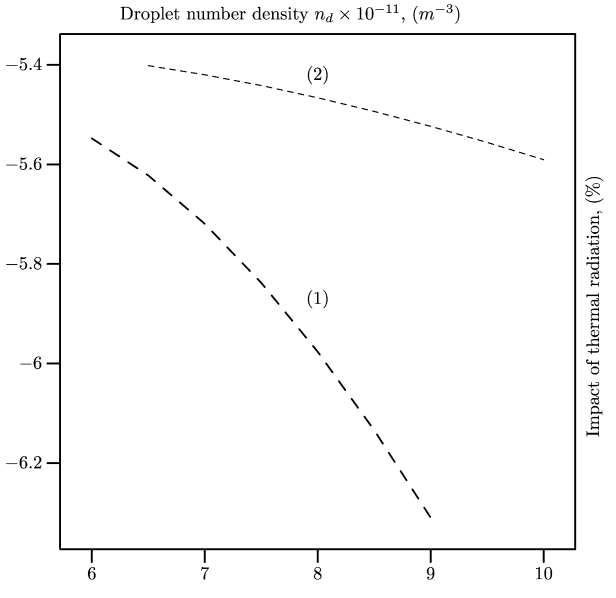

Fig. 15. Impact of Thermal Radiation versus droplets number density as predicted by Eq. (36) for $T_{\text{ext}} = 2500$ K and $T_{g0} = 750$ K ((1) refers to $R_{d0} = 12$ μm, (2) refers to $R_{d0} = 9.5$ μm).

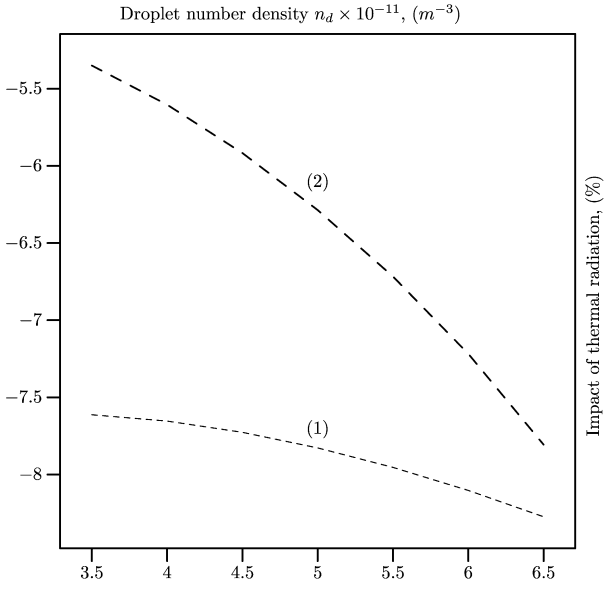

Fig. 16. The same as Fig. 15 but for $T_{g0} = 775$ K, $T_{\text{ext}} = 2500$ K.

but not unrealistic. As in the case discussed in Section 4.4, this temperature can be assumed to be linked with the temperature of remote flames. As can be seen from these figures, the delay time increases with increasing droplet number density and radius, and decreases with increasing initial gas temperature. This is consistent with the results shown in Figs. 9 and 10. The physical explanation of these dependencies is the same as given in Section 4.4 for the case when gas temperature is a fast variable.

Figs. 15 and 16 show the dependence of the thermal radiation impact on the droplets number density for the same values of parameters as in Figs. 13 and 14. As in the case discussed in Section 4.4, the impact of thermal radiation shown in Figs. 15 and 16 is always negative, which indicates that thermal radiation leads to decrease in the ignition delay time, Also, similarly to the case considered in Section 4.4, the impact of thermal radiation increases with increasing droplet number density and droplet radii, and decreasing initial gas temperature. The physical explanation of all these properties is the same as given in Section 4.4.

The absolute values of impact of thermal radiation shown in Figs. 15 and 16 are much less than shown in Figs. 11 and 12. This can be attributed to two factors. Firstly the sizes of droplets for which Figs. 15 and 16 are presented are much less than those used for Figs. 11 and 12 (the amount of thermal radiation energy absorbed in droplets is approximately proportional to their radii in the power 2.5 [23,24]). Secondly, in the case considered

in this section, part of the ignition delay is due to the induction time, on which the thermal radiation has no influence.

Note that the total ignition delays shown in Figs. 13 and 14 are somewhat less than those predicted in [6]. This can be attributed to different values of coefficients in the chemical terms and different approximations used in the present model and in [6] (see the discussion in Section 4.4). The decrease of the ignition delay time with increasing initial gas temperature, which follows from Figs. 13 and 14, is consistent with Fig. 5 of [6].

The order of magnitude of the total ignition delay predicted by the present model and the model described in [6] agree with experimental data and predictions from CFD simulations [18,19].

4. Conclusions

A new model, taking into account the oxidizer and thermal radiation effects on the thermal explosion of a hot combustible mixture of air and evaporating fuel droplets is presented. The analysis is performed for the values of parameters typical for diesel engines-like environments. The physical properties of the fuel are taken those for *n*-dodecane, except for the spectrum of the thermal radiation absorption which was based on the direct measurements for low sulphur ESSO AF1313 diesel fuel as reported in [8]. The droplets are assumed to be semi-transparent, and their heating is controlled by the external temperature (associated with remote flames). The model takes into account the heat release due to the exothermic oxidation of fuel vapour, heat losses due to liquid fuel evaporation, fuel vapour consumption as a result of a chemical reaction, fuel vapour supply by evaporated liquid fuel and two mechanisms of heating of evaporating fuel droplets: convection and radiation. The system of equations describing the effects of heating, evaporation and combustion of fuel droplets is simplified by assuming that the Nusselt and Sherwood numbers are equal to 2. Also, the effects of the Stefan flow on heating and evaporation are ignored by assuming that Spalding mass and temperature numbers are small. The mathematical formulation of the problem is presented in the form of a singularly perturbed system of four nonlinear ordinary differential equations. The dynamical behavior of the system is investigated with the help of the geometrical version of the method of integral manifolds (MIM). It is shown that this method is applicable in the cases when gas or droplet temperatures are fast variables in the system. The subranges of parameters when these regimes can take place are identified.

In the case when the droplet temperature is identified as the fast variable, the ignition time delays are presented as a sum of the physical delay (heat-up and evaporation time) and the chemical delay (induction time). During the droplet heat up and evaporation period the leading-order solution indicated the synchronization between the temperature of the droplets, their radius, and gas temperature. The analytical expressions for the heat-up and evaporation delay time and induction delay time are derived. The dependence of both delays on the physical parameters of the system is investigated.

In both cases the total ignition delay time and the absolute value of the thermal radiation impact increase with the increase of the droplet number density and radii. Also, in both cases the increase of the initial gas temperature leads to the decrease of the total ignition delay and the impact of thermal radiation. The thermal radiation effects lead to a decrease in the total ignition delay time, as follows from the negative values of the impact of thermal radiation. The absolute values of the impact of thermal radiation are noticeably greater when compared with the case studied in [6], where it was assume that the external temperature is equal to the current gas temperature.

References

[1] K.K. Kuo, Principles of Combustion, Wiley, New York, 1986.
[2] S.K. Aggrawal, A review of spray ignition phenomena: present status and future research, Progr. Energy Combust. Sci. 24 (1998) 565–600.
[3] V.I. Babushok, V.M. Gol'dshtein, Structure of the thermal explosion limit, Combust. Flame 72 (1988) 211–216.
[4] V.M. Gol'dshtein, V.A. Sobolev, Singularity theory and some problems of functional analysis, AMS Translations 153 (1992) 73–92.
[5] S. Sazhin, G. Feng, M. Heikal, I. Goldfarb, V. Goldshtein, G. Kuzmenko, Thermal ignition analysis of a monodisperse spray with radiation, Combust. Flame 124 (2001) 684–701.
[6] I. Goldfarb, S. Sazhin, A. Zinoviev, Delayed thermal explosion in flammable gas containing fuel droplets: asymptotic analysis, J. Engrg. Math. 50 (2004) 399–414.
[7] L.A. Dombrovsky, S.S. Sazhin, E.M. Sazhin, G. Feng, M.R. Heikal, M.E.A. Bardsley, S.V. Mikhailovsky, Heating and evaporation of semi-transparent diesel fuel droplets in the presence of thermal radiation, Fuel 80 (2001) 1535–1544.
[8] S.S. Sazhin, W.A. Abdelghaffar, E.M. Sazhin, S.V. Mikhailovsky, S.T. Meikle, C. Bai, Radiative heating of semi-transparent diesel fuel droplets, ASME J. Heat Transfer 126 (2004) 105–109, 490–491.
[9] I. Goldfarb, V. Gol'dshtein, A. Zinoviev, Delayed thermal explosion in porous media: method of invariant manifolds, IMA J. Appl. Math. 67 (2002) 263–280.
[10] S.S. Sazhin, Advanced models of fuel droplet heating and evaporation, Progr. Energy Combust. Sci. 32 (2006) 162–214.
[11] L.A. Dombrovsky, S.S. Sazhin, Absorption of external thermal radiation in asymmetrically illuminated droplets, J. Quantitative Spectrosc. Radiation Transfer 87 (2) (2004) 119–135.
[12] L.A. Dombrovsky, Spectral model of absorption and scattering of thermal radiation by diesel fuel droplets, High Temperature 40 (2) (2002) 242.
[13] L.A. Dombrovsky, L.I. Zaichik, Conditions of thermal explosion of a radiating gas with polydisperse liquid fuel, High Temperature 39 (2001) 604–611.
[14] Ju.A. Mitropolskii, O.B. Likova, Integral Manifolds in Nonlinear Mechanics, Nauka, Novosibirsk, 1973.
[15] N. Fenichel, Geometric singular perturbation theory for ordinary differential equations, J. Diff. Eq. 31 (1979) 53–98.
[16] B.B. Strygin, V.A. Sobolev, Decomposition of Motions by the Integral Manifolds Method, Nauka, Moscow, 1988.
[17] N.N. Semenov, Zur theorie des verbrennungsprozesses, Z. Phys. Chem. 48 (1928) 571–581.
[18] E.M. Sazhina, S.S. Sazhin, M.R. Heikal, V.I. Babushok, R.A. Johns, A detailed modelling of the spray ignition process in diesel engines, Combust. Sci. Technol. 160 (2000) 317–344.
[19] P.F. Flynn, R.P. Durrett, G.L. Hunter, A.O. zur Loye, O.C. Akinyemi, J.E. Dec, C.K. Westbrook, Diesel combustion: an integrated view combining laser diagnostics, chemical kinetics, and empirical validation, SAE Report 1999-01-0509, 1999.
[20] S.S. Sazhin, E.M. Sazhina, M.R. Heikal, C. Marooney, S.V. Mikhailovsky, The shell autoignition model: a new mathematical formulation, Combust. Flame 117 (1999) 529–540.

[21] E.M. Sazhina, S.S. Sazhin, M.R. Heikal, C. Marooney, The shell autoignition model: application to gasoline and diesel fuels, Fuel 78 (4) (1999) 389–401.
[22] C.K. Westbrook, F.L. Dryer, Simplified reaction mechanism for the oxidation of hydrocarbon fuels in flames, Combust. Sci. Technol. 27 (1981) 31–43.
[23] B. Abramzon, S. Sazhin, Droplet vaporization model in the presence of thermal radiation, Int. J. Heat Mass Transfer 48 (2005) 1868–1873.
[24] B. Abramzon, S. Sazhin, Convective vaporization of fuel droplets with thermal radiation absorption, Fuel 85 (2005) 32–46.